Van Eldik, L. J., Watterson, D. M., Fok, K.-F., & Erickson, B. F. (1983b) *Arch. Biochem. Biophys. 227*, 522–533.
Wallace, R. W., & Cheung, W. Y. (1979) *J. Biol. Chem. 254*, 6564–6571.
Walsh, M., Stevens, F. C., Kuznicki, J., & Drabikowski, W. (1977) *J. Biol. Chem. 252*, 7440–7443.
Watanabe, Y., & Nozawa, Y. (1982) in *Calcium and Cell Function* (Cheung, W. Y., Ed.) Vol. 2, pp 297–324, Academic Press, New York.
Watterson, D. M., & Vanaman, T. C. (1976) *Biochem. Biophys. Res. Commun. 73*, 40–46.
Watterson, D. M., Harrelson, W. G., Jr., Keller, P. M., Sharief, F., & Vanaman, T. C. (1976) *J. Biol. Chem. 251*, 4501–4513.
Watterson, D. M., Sharief, F., & Vanaman, T. C. (1980) *J. Biol. Chem. 255*, 962–975.
Watterson, D. M., Burgess, W. H., Lukas, T. J., Iverson, D., Marshak, D. R., Schleicher, M., Erickson, B. W., Fok, K.-F., & Van Eldik, L. J. (1984) *Adv. Cyclic Nucleotide Res. 16*, 205–226.
Yazawa, M., Yagi, K., Toda, H., Kondo, K., Narita, K., Yamazaki, R., Sobue, K., Kakiuchi, S., Nagao, S., & Nozawa, Y. (1981) *Biochem. Biophys. Res. Commun. 99*, 1051–1057.

Submicrosecond and Microsecond Rotational Motions of Myosin Head in Solution and in Myosin Synthetic Filaments As Revealed by Time-Resolved Optical Anisotropy Decay Measurements†

Kazuhiko Kinosita, Jr., Shin'ichi Ishiwata,* Hideyuki Yoshimura,‡ Hiroshi Asai, and Akira Ikegami

ABSTRACT: Rotational Brownian motions of the head portion (subfragment 1) of rabbit skeletal myosin were studied by the measurement of flash-induced absorption anisotropy decay and phosphorescence anisotropy decay of the triplet probe 5-eosinylmaleimide bound to the myosin head. Fluorescence anisotropy decay of the fluorescent probe *N*-(1-pyrenyl)maleimide was also examined in some cases. Most of the triplet signals were observed in the presence of 60% (w/w) sucrose, which simply reduced the rate of motion via viscosity damping, to obtain good time resolution. Anisotropy decay of eosin on isolated head fragment was single exponential over two decades; the data indicated that the largest diameter of the head was 14–17 nm if the head was modeled as a prolate ellipsoid of revolution and 12–13 nm if oblate. Anisotropy decay in myosin synthetic filaments consisted of a fast and a slow component and a small constant part; myosin monomers and heavy meromyosin gave similar but somewhat faster decays with a smaller residual anisotropy. For each sample, the decay curves between −10 and 30 °C overlapped with each other after reducing the time scale to that at 20 °C in the absence of sucrose, showing that no gross conformational changes occurred between these temperatures. The fast decay was in the submicrosecond range on the reduced time scale and could be explained by a wobbling motion of the head around the head–rod junction within a cone of semiangle 35° for filament and 41° for solubilized proteins. The slow decay had a relaxation time of a few microseconds and indicated that a part of the rod portion next to the head also wobbled extensively. Analysis in which the rod end was assumed to wobble uniformly in a cone suggested that the effective length of the wobbling part was about 14 nm, and the cone angle was estimated to be about 48° in filament and 57–60° for solubilized proteins.

The molecular mechanism of muscle contraction is not yet fully understood. In striated muscles of vertebrates, sliding motion of the thick and thin filaments past each other leads to contraction (Huxley & Niedergerke, 1954; Huxley & Hanson, 1954), although shortening of the filaments themselves might also take place under certain conditions [see review by Pollack (1983)]. During contraction, the cross bridges projecting from the thick (myosin) filament approach the thin (actin) filaments; the force pulling the two sets of filaments against each other is apparently mediated by the cross bridges (Huxley, 1969). Where and how the force is generated, however, are still challenging problems.

A prevailing model has been one in which a cross bridge first attaches to an actin filament with a certain angle of tilt and subsequently changes the tilt angle, generating tension in an elastic arm which connects the bridge to the backbone of the myosin filament; after tension is exerted, the cross bridge is detached from the actin filament for the next cycle of reaction (Huxley, 1969; Huxley & Simmons, 1971). Recent studies, however, do not necessarily support this model, at least in its simplest form: Attempts at finding a variation in the angle of attachment of cross bridges using fluorescence (Yanagida, 1981) or electron paramagnetic resonance (Cooke et al., 1982) have revealed a rather uniform tilt, contrary to expectation from the model. Three-dimensional analyses of electron micrographs (Wakabayashi & Toyoshima, 1981) have shown a tilt angle different from a previously suggested one (Reedy et al., 1965) upon which the model was based. Clearly more information, particularly about dynamic aspects, is needed before a final answer is reached.

Two aspects should be distinguished when one considers the molecular dynamics of muscle contraction. One is the "conformational change(s)" of participating molecules: a different equilibrium structure may be induced when a protein

† From the Institute of Physical and Chemical Research, Hirosawa 2-1, Wako-shi, Saitama 351-01, Japan (K.K., H.Y., and A.I.), and the Department of Physics, School of Science and Engineering, Waseda University, 3-4-1 Okubo, Shinjuku-ku, Tokyo 160, Japan (S.I. and H.A.).
Received May 23, 1984. This work was supported in part by Grants-in-Aid from Ministry of Education, Science and Culture of Japan and in part by special coordination funds for the promotion of science and technology and a research grant for "Solar Energy-Photosynthesis" given by the Agency of Science and Technology of Japan.
‡ Present address: Biometrology Laboratory, JEOL Ltd., Nakagami, Akishima, Tokyo 196, Japan.

0006-2960/84/0423-5963$01.50/0

molecule interacts with another or when it binds a ligand. The other is thermal fluctuation around an equilibrium structure. Description of molecular events as conformational changes is common. However, the possible significance of thermal fluctuation should also be borne in mind.

A particularly instructive model in this regard has been one proposed by Huxley (1957), where thermal energy is postulated to be the primary source of the contraction force. Although later experiments led to a major revision of the model (Huxley & Simmons, 1971, 1972), it is very probable that part of the contraction cycle is mediated by thermal motions of muscle proteins. Extensive and rapid thermal fluctuations, which we report in this article, not only augment this possibility but also warn against those models which describe the contraction events as a series of changes in more or less well-defined conformations.

Another important role of thermal motions, for researchers, is that they offer valuable information about the dynamic structure of molecules or supramolecular architectures (Fujime & Ishiwata, 1971; Ikegami et al., 1983; Kinosita et al., 1984). In general, the rate of thermal fluctuation in a medium of known viscosity is related to the size of the moving unit (irrespective of whether the motion is free or restricted by a potential). Compared to translation, rotational Brownian motion is particularly sensitive to size. Flexibility or the existence (and possibly the location) of a swivel junction, for example, can thus be easily demonstrated by comparing the size determined from the rate of rotational motion with the geometrical size estimated, e.g., from molecular weight or by electron microscopy. If, on the other hand, the range of thermal motion is limited, it implies a potential barrier, for example, a "spring" that holds the moving unit. The width of the potential well, or the strength of the spring, may be estimated from the analysis of thermal motion.

We report below the motion of myosin heads, the two globular parts attached to the long rod portion in the Y-shaped myosin molecule. The head contains actin-binding site(s) and corresponds to, or is a part of, the cross bridge. To observe the motion of the head, we selectively labeled the fast reacting thiol (SH_1)[1] in the head with either the fluorescent probe *N*-(1-pyrenyl)maleimide (PMI) or the triplet probe 5-eosinylmaleimide (EMI). We excited the probe molecules with polarized, pulsed light and followed the decay of anisotropy of the flash-induced optical signal, either fluorescence, transient absorption, or phosphorescence. The anisotropy decay reflected the change in orientation of the probe molecule, and therefore of the myosin head, with time. The rotational motion of the isolated head, the subfragment 1 (S1) obtained by chymotryptic digestion, indicated that S1 was rigid and its long axis was about 16 nm. In myosin synthetic filaments, whose structure we suppose to be very similar to that of the thick filaments [a review by Koretz (1982)], the head underwent an extensive wobbling motion over many tens of degrees in a time range on the order 1 μs. The wobbling motion of the head could not be explained by the presence of a single swivel between the head and the rod portion; analysis suggested that part of the rod closer to the head also wobbled quite extensively and rapidly.

The head motion has already been studied by Mendelson, Morales, and co-workers (Mendelson et al., 1973; Mendelson & Cheung, 1976, 1978) using the fluorescence depolarization technique. Our present study is an extension of their work. The probe used in the early studies, however, was 5-[[2-[(iodoacetyl)amino]ethyl]amino]naphthalene-1-sulfonic acid (IAEDANS) having a fluorescence lifetime of only about 21 ns, much too short to fully explore the head wobbling that extends into the microsecond time range. Our triplet probe eosin, in contrast, had a lifetime of a few milliseconds and thus allowed a detailed and less ambiguous analysis of the dynamic structure of the myosin filament. Rapid rotation of the myosin head has also been suggested by saturation-transfer EPR studies (Thomas et al., 1980; Thomas et al., 1983). With the EPR technique that is not time resolved, however, quantitative analysis is difficult unless the mode of rotation is known to be the simplest one. The present study enjoys both the time-resolving capability and broad time window of the triplet technique, key requirements for an analysis of complex rotational motions as exhibited by the myosin head.

Materials and Methods

Chemicals. PMI and EMI were purchased from Molecular Probes and used without further purification in most experiments. Thin-layer chromatography on silica gel with chloroform–methanol (3:2 by volume) showed that the purity of EMI was 90%. Before some experiments, EMI was partially purified to 96% with a Sephadex LH20 column by using the same solvent. (Later we found that an SiO_2 column, Merck SI60, worked better.) However, the triplet signals were indistinguishable from other results. ATP was purchased from Boehringer Mannheim Co. and α-chymotrypsin from Worthington Biochemical Co. Other chemicals were of reagent grade.

Preparation of Myosin. Myosin was prepared from rabbit back and leg white muscle according to Perry (1955) with the following slight modifications: The incubation time in a Guba-Straub solution was 10 min instead of 15 min. Also, at the final stage of purification, myosin solution was ultracentrifuged at 100000*g* for 3 h in 0.3 M KCl, and the precipitate was discarded. Purified myosin was stored at −20 °C in 50% (v/v) glycerol, 0.25 M KCl, and 5 mM potassium phosphate buffer (pH 6.7).

Labeling Procedures. After glycerol was removed, myosin filaments (10 mg/mL = 21 μM) were mixed with 40 μM of PMI or EMI in 50 mM KCl, 5 mM MOPS (pH 7.0), and 0.1 mM EDTA. Three minutes later, the reaction was stopped by adding 1 mM dithiothreitol, and the solution was centrifuged at 600*g* for 10 min. The sedimented filaments were dissolved in 0.5 M KCl, 5 mM MOPS (pH 7.0), and 0.1 mM EDTA. Filaments were then re-formed by lowering the KCl concentration to 50 mM and recollected by centrifugation. The cycle of dissociation–association was repeated 6–7 times until unbound dye disappeared. Finally, myosin aggregates undissolved in the 0.5 M KCl solution described above were removed by ultracentrifugation at 100000*g* for 2 h. All procedures were performed at 0 °C in the dark.

Preparation of Myosin Filaments and Subfragments. Myosin synthetic filaments were prepared by dialyzing the labeled myosin in 0.5 M KCl, 5 mM MOPS (pH 7.0), and 0.1 mM EDTA against 0.1 M KCl, 10 mM MOPS (pH 7.0), and 0.1 mM EDTA at 0 °C. Heavy meromyosin (HMM) and S1 were prepared from labeled or unlabeled myosin according to Weeds & Pope (1977); digestion with α-chymotrypsin was carried out in 0.6 M NaCl, 20 mM MOPS (pH 7.0), and 1 mM $MgCl_2$ for HMM and in 0.12 M NaCl, 20 mM MOPS

[1] Abbreviations: EDTA, ethylenediaminetetraacetic acid; EMI, 5-eosinylmaleimide; EPR, electron paramagnetic resonance; HMM, heavy meromyosin; IAEDANS, 5-[[2-[(iodoacetyl)amino]ethyl]amino]-naphthalene-1-sulfonic acid; MOPS, 3-(*N*-morpholino)propanesulfonic acid; PMI, *N*-(1-pyrenyl)maleimide; SH_1, the fast reacting thiol of myosin; S1, myosin subfragment 1; Tris, tris(hydroxymethyl)aminomethane; ATPase, adenosinetriphosphatase.

Table I: Distribution of EMI Label among Myosin Subfragments

	mol of EMI/mol of protein (distribution in %)		
	myosin	S1	rod
sample 1	1.90 (100)	0.88 (93)	0.17 (9)
sample 2	1.26 (100)	0.57 (90)	0.09 (7)

(pH 7.0), and 1 mM EDTA for S1. Myosin rod was prepared from the residue of S1 preparation as follows. After the residue was dissolved in 0.6 M KCl and 10 mM Tris–maleate buffer (pH 6.8), three volumes of ethanol were added. Three hours later, the precipitate was collected by filtering the solution with gauze, and the material was dialyzed against 0.5 M KCl and 10 mM MOPS (pH 7.0). Undissolved proteins including denatured myosin were removed by ultracentrifugation at 100000g for 2 h. The supernatant was used as a rod fraction. All procedures were performed at 0 °C in the dark.

Degree of Labeling and Distribution among Subfragments. The concentrations of the dyes bound to myosin and its subfragments were determined from the absorbance at the main peak (around 530 nm for EMI and 343 nm for PMI). The extinction coefficients used were 8×10^4 M^{-1} cm^{-1} for EMI (Cherry, 1978) and 3.75×10^4 M^{-1} cm^{-1} for PMI (Holowka & Hammes, 1977). The protein concentrations were determined from the absorbance at 280 nm after appropriate corrections for the contribution from the bound dye. The extinction coefficients used were 0.53 (L/g) cm^{-1} for myosin, 0.81 (L/g) cm^{-1} for S1, 0.60 (L/g) cm^{-1} for HMM, and 0.22 (L/g) cm^{-1} for rod (Margossian & Lowey, 1982). Molar concentrations of these proteins were calculated from the assumed molecular weights of 4.8×10^5 for myosin (Tonomura et al., 1966), 1.15×10^5 for S1 (Lowey et al., 1969), 3.5×10^5 for HMM, and 2.2×10^5 for rod (Margossian & Lowey, 1982). A biuret method (Gornall et al., 1949) at 540 nm and a modified Lowry method (Ohnishi & Barr, 1978) at 750 nm for EMI-labeled proteins gave results consistent with the ultraviolet absorption.

For several preparations used in the present study, the molar ratio of bound EMI to myosin estimated from the above concentrations ranged between 1.2 and 1.9. Table I shows examples with high and low degrees of labeling. In both samples, about 90% of bound EMI was found in S1. This was the case for other preparations as well. The variation in the amount of bound dye did not affect the anisotropy decay. Labeling of PMI was done in one preparation, which gave PMI to S1 molar ratio of 0.12. Label distribution was not determined because only S1 was used for fluorescence measurements.

Gel Electrophoresis. Polyacrylamide slab gel electrophoresis in the presence of sodium dodecyl sulfate was performed according to Laemmli (1970) with slight modifications. Acrylamide concentrations of 15% and 5% were used for a separation gel and a stacking gel, respectively. Samples were prepared by dialyzing protein solutions (about 1 mg/mL) against 1% sodium dodecyl sulfate, 1% β-mercaptoethanol, and 10 mM Tris-HCl (pH 6.8) for 1 or 2 days at room temperature. Figure 1 shows that EMI was selectively incorporated into the heavy chains of myosin and S1.

ATPase Assays. The ATPase activities of myosin and its subfragments were measured at 25 °C, according to Ohnishi et al. (1975), from the rate of liberation of inorganic phosphate. Results for a typical preparation are shown in Table II. The labeling with EMI induced an increase in Ca^{2+}–ATPase and a concomitant decrease in K^+–EDTA–ATPase, indicating the modification of the most reactive thiols of myosin, SH_1 (Sekine & Kielley, 1964). The extent of SH_1 modification, estimated from the fractional decrease in the K^+–EDTA–ATPase activity, agreed within experimental error with the degree of labeling. Thus, most of the bound EMI appears to be at SH_1.

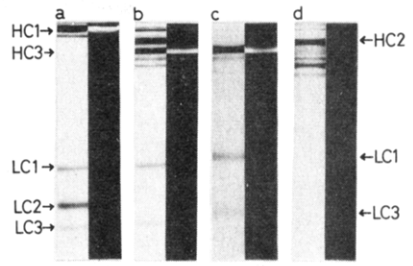

FIGURE 1: Sodium dodecyl sulfate–polyacrylamide gel electrophoresis of EMI–myosin and its subfragments (sample 1 in Table I). (a) EMI–myosin; (b) EMI–myosin digested with chymotrypsin for 10 min; (c) purified S1 obtained from EMI–myosin; (d) rod fraction from EMI–myosin. In each pair of photographs, the left lane shows proteins stained with Coomassie brilliant blue, and the right lane shows EMI fluorescence before the staining. In (b) EMI–myosin (10 mg/mL) was incubated at 25 °C in the presence of 0.05 mg/mL α-chymotrypsin in 0.12 M NaCl, 20 mM MOPS (pH 7.0), and 1 mM EDTA. After 10 min, 50 μL of the sample was mixed with 200 μL of a solution containing 1.25% sodium dodecyl sulfate, 1.25% β-mercaptoethanol, and 12.5 mM Tris-HCl (pH 6.8) at 80 °C. The solution was left overnight at room temperature and applied to the gel. Symbols HC1, HC2, and HC3 indicate the bands of heavy chains of myosin, rod, and S1, respectively. LC1, LC2, and LC3 show light chains.

Table II: ATPase Activities of Labeled Myosin at 25 °C[a]

	unmodified myosin	EMI–myosin	EMI–S1
Ca^{2+}–ATPase[b]	110 (10)	210 (20)	140 (20)
K^+–EDTA–ATPase[c]	950 (50)	360 (30)	170 (30)
% SH_1 modified	0	62 (5)	64 (8)

[a] In this preparation, molar ratios of EMI to protein were 1.51 for myosin (0.76 per head) and 0.69 for S1. The numbers in parentheses show the range for the results of two sets of measurements. [b] Units: μmol of phosphate/(μmol of protein·min). In 0.6 M KCl, 5 mM ATP, 50 mM Tris-HCl (pH 7.5), and 10 mM $CaCl_2$. [c] Units: μmol of phosphate/(μmol of protein·min). In 0.45 M KCl, 5 mM ATP, 50 mM Tris-HCl (pH 7.5), and 1 mM EDTA.

Apparatus for Measurements of Phosphorescence and Absorption Anisotropy Decays. The principle of triplet anisotropy decay measurements has been reviewed (Cherry, 1978; Ando, 1978; Jovin et al., 1981). Figure 2 shows an optical diagram of our apparatus, with which we can measure both phosphorescence and absorption signals.

The excitation source was either a flash-lamp-pumped dye laser (Phase-R, Model DL-1400) or an Nd/YAG laser (Quanta-Ray, Model DCR-2A); the respective results were indistinguishable. Untuned emission from the dye laser operated at 2 Hz with a dye Green 9 (coumarin 540AF) in ethanol was at a wavelength of 540 nm and had a nominal pulse duration of 250 ns; temperature control via a Triax adapter was found essential for a stable operation. The Nd/YAG laser with a nominal pulse duration of 25 ns was operated at 30 Hz, and the second harmonic at 532 nm was used for excitation after passage of the beam through a quarter-wave plate. The excitation beam from either laser was dispersed by a set of lenses to reduce the intensity and to improve the beam homogeneity. Further reduction of the intensity, when necessary, was achieved with Zeiss neutral density filters. The beam was then polarized vertically or horizontally with a Glan prism. The beam intensity at the sample was set so that at most a few percent of the dye molecules in the illuminated region (beam cross section 8×8 mm^2) went to the excited triplet state, as judged from the

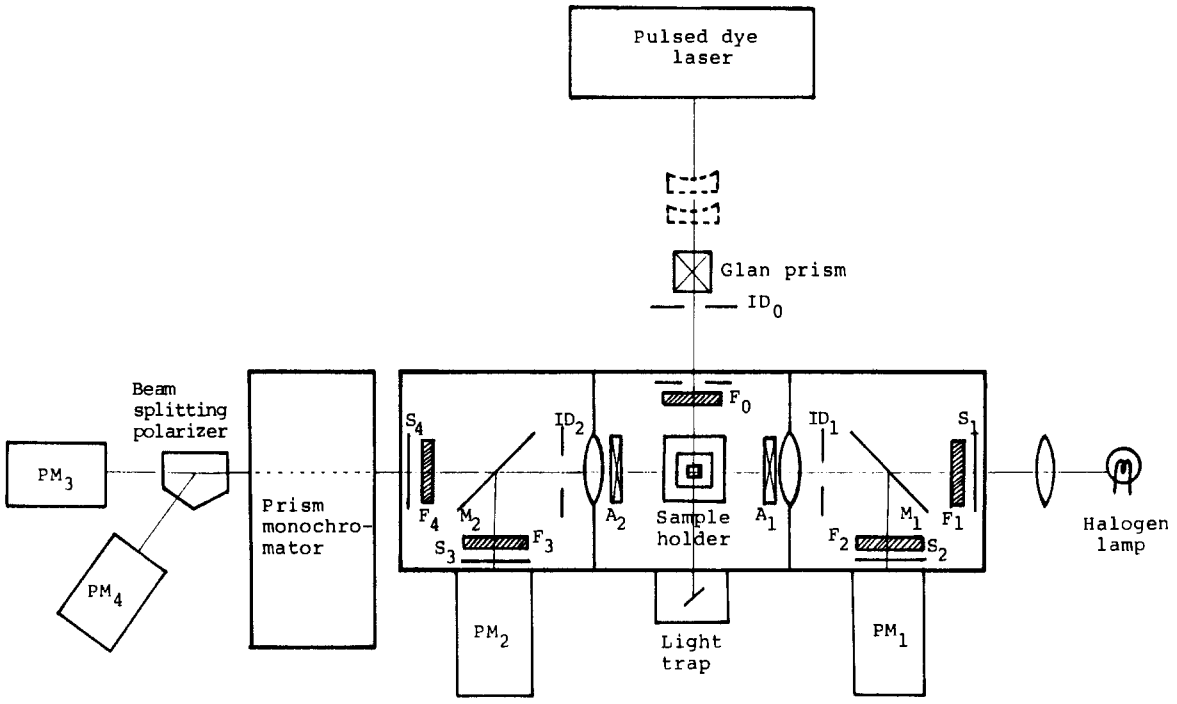

FIGURE 2: Optical diagram of the apparatus for triplet anisotropy decay measurements. ID, iris diaphragm; S, solenoid-driven shutter; F, optical filters; M, mirror; A, polarization analyzer; PM, photomultiplier tube.

absorption signal. The intensity of the Nd/YAG beam was kept particularly low, since the beam was noticeably inhomogeneous even after the dispersion lenses.

The temperature-controlled sample holder was designed so as to accommodate a cuvette with different sizes at various positions. In the present study, we used a 1 × 1 cm^2 cuvette with a rubber cap, which was placed at the center of the sample holder in phosphorescence measurements; for absorption, the cuvette was displaced so that the measuring beam, 2 mm wide and 8 mm high, went through the front (laser side) edge of the sample. The sample temperature was monitored with a thermocouple immersed in the sample. During low-temperature measurements, the entire sample compartment was flushed with nitrogen gas.

In phosphorescence measurements, the laser-induced emission was passed through a pair of sheet polarizers A_1 and A_2 (Polaroid HNP'B), one vertically and the other horizontally oriented, and directed by mirrors M_1 and M_2 to Hamamatsu R1333 photomultiplier tubes, which were gated off during the laser illumination by a circuit provided by Hamamatsu Photonics (C1392-01). Emission above 660 nm was selected with Fuji-Film SC62 and SC66 sharp-cut filters.

The measuring beam for absorption measurements was provided by a quartz–halogen lamp (Osram 64625, DC 100 W); a multicavity interference filter (Koshin Kogaku Co., Ltd.) and a Hoya C500 heat absorbing filter selected green light between 489 and 522 nm with sharp cutoffs. Mirrors M_1 and M_2 and analyzers A_1 and A_2 were removed. Unnecessary exposure of the sample to the measuring beam was avoided with a solenoid-driven shutter, S_1. After passing through the sample, the beam passed through two green interference filters described above and then through a Zeiss prism monochromator with a band-pass of 19 nm; the monochromator was set at 515 nm to observe the ground-state depletion signal of eosin. The combination completely blocked scattered laser light. The beam was finally divided into vertically and horizontally polarized components with a beam-splitting polarizer (Karl Lambrecht, SBTA-12-45 with KL-2 U.V. option) and led to Hamamatsu R374 photomultiplier tubes in which the last seven dynodes were connected to the anode. A piece of sheet polarizer was placed before each photomultiplier tube to ensure the quality of polarization.

In both phosphorescence and absorption measurements, the anode of each photomultiplier tube was connected with a short coaxial cable to a Tektronix AM502 amplifier with an input impedance internally reduced to 10 kΩ and with a gain fixed to 100×. The output was fed to a homemade signal processor (made of Analog Devices AD528 operational amplifiers), where signals for the vertically and horizontally polarized components, i_V and i_H, were separately amplified with variable gains (5× to 10×) and then combined to produce $i_D \equiv i_V - i_H$ and $i_T \equiv i_V + 2i_H$. The signals i_D and i_T were digitized and averaged with a Nicolet 1170 signal averager with a 172/4B plugin (12 bits; minimum channel separation 2 μs under dual-input operation) and finally transferred to a DEC LSI-11/02 or LSI-11/23 microcomputer for data processing and analysis. The reasons for the analog processing into i_D and i_T were (a) to ensure a good precision for i_D, (b) to help judge the data by eye during accumulation, and (c) to enable immediate display of the anisotropy decay using the division capability of the averager.

Measuring Procedures. Prior to a triplet measurement, oxygen in the sample was removed by the following procedure: First, a desired medium (>80% of the final volume), without protein, was introduced into a cuvette containing a stir piece (a hollow cube with the top face removed and the bottom face perforated with several holes that allowed the passage of water; made of glass and contained a piece of kovar). Sucrose, when desired, was added at this stage from a fresh, supersaturated stock solution (75% w/w) in an appropriate buffer. After the solution was degassed under reduced pressure, a sample containing labeled protein was gently placed on top of the solution and the cuvette sealed with a rubber cap. Argon gas was blown onto the sample through a needle, without bubbling, while the sample was gently agitated with slow (≈0.2 Hz) up-and-down strokes of the stir piece driven by external magnets.

After 10–20 min, the cuvette was placed in the sample holder, and the amplifier gains were adjusted so as to give the

same overall sensitivities for i_V and i_H: In phosphorescence, the signal $i_D(t) = i_V(t) - i_H(t)$ displayed on the averager was nullified for horizontally polarized excitation. In absorption, the two DC signals i_V and i_H displayed on panel meters were equalized, and then the inputs to the signal processor were changed into the AC-coupling mode. After the adjustment, transient signals $i_D(t)$ and $i_T(t)$ were accumulated over 256–2048 shots in separate 512-channel memories in the averager; signals for both vertically and horizontally polarized excitations were recorded to produce altogether four traces for each sample. Trigger signals for the laser, averager, and gating circuit for the phosphorescence photomultiplier tubes were generated by a master controller; the laser trigger was delayed so that the transient signals were preceded by about 50 channels of flat region, from which the base line was calculated.

Data Processing and Analysis. First, the base-line level was subtracted from each trace. Then, traces $i_D(t)$ and $i_T(t)$ for horizontally polarized excitation were integrated over the entire time window to calculate the ratio S between the sensitivities for the vertically and horizontally polarized light components:

$$\left[\int i_D(t)dt / \int i_T(t)dt\right]_{\text{horiz excit}} = (S - 1)/(S + 2) \quad (1)$$

Since the amplifier gains had previously been adjusted, deviation of S from one was small and at most a few percent in the worst case. However, checking the value of S was important in the absorption measurements, because fatigued photomultiplier tubes showed some discrepancy between static and dynamic gains, resulting in a significant deviation of S from one; such tubes were replaced. Performance of the apparatus was also checked occasionally with the purple membrane of *Halobacterium halobium* as a sample, which gave an anisotropy close to the theoretical maximum (Kouyama et al., 1981).

Traces $i_D(t)$ and $i_T(t)$ for vertically polarized excitation were recombined to reproduce $i_V(t)$ and $i_H(t)$, and the latter was corrected for S:

$$I_V(t) = i_V(t) \qquad I_H(t) = Si_H(t) \quad (2)$$

Since S was close to one, precision in the difference signal was preserved. In phosphorescence measurements, the total phosphorescence intensity $I_T(t)$ and anisotropy $r(t)$ were calculated as

$$I_T(t) = I_V(t) + 2I_H(t) \qquad r(t) = [I_V(t) - I_H(t)]/I_T(t) \quad (3)$$

In absorption, $I_V(t)$ and $I_H(t)$ were first converted to absorbance changes $\Delta A_V(t)$ and $\Delta A_H(t)$, from which the total absorbance change $\Delta A_T(t)$ and anisotropy $r(t)$ were calculated:

$$\Delta A_V(t) = -\log [1 + I_V(t)/I_S]$$
$$\Delta A_H(t) = -\log [1 + I_H(t)/I_S] \quad (4)$$

$$\Delta A_T(t) = [\Delta A_V(t) + 2\Delta A_H(t)]/3$$
$$r(t) = 3[\Delta A_V(t) - \Delta A_H(t)]/\Delta A_T(t) \quad (5)$$

where I_S is the DC light level before excitation. The quantities $I_T(t)$ and $\Delta A_T(t)$ are proportional to the number of molecules in the excited triplet state, and $r(t)$ reflects rotational motion.

To characterize the experimental decays, $I_T(t)$, $\Delta A_T(t)$, and $r(t)$ were fitted with the following functions by using a least-squares program:

$$I_T(t) = I_0 \sum_{i=1}^{N} \alpha_i \exp(-t/\tau_i) \qquad \sum_{i=1}^{N} \alpha_i = 1 \quad (6)$$

$$\Delta A_T(t) = A_0 \sum_{i=1}^{N} \alpha_i \exp(-t/\tau_i) \qquad \sum_{i=1}^{N} \alpha_i = 1 \quad (7)$$

$$r(t) = r_0 \sum_{j=1}^{M} \beta_j \exp(-t/\phi_j) \qquad \sum_{j=1}^{M} \beta_j = 1 \quad (8)$$

Analyses for $I_T(t)$ and $\Delta A_T(t)$ were routinely carried out for $N = 1$ and 2. For $r(t)$, analyses with $M = 2$ and 3 were tried with ϕ_M fixed to infinity, except for the data on S1 where M was set to 1. In some analyses, r_0 was fixed to a predetermined value as described under Results.

Triplet Anisotropy Values. In addition to statistical errors (including variations in samples), the triplet absorption measurements with intense laser excitation suffered from the saturation effect (Lachish et al., 1976; Kawato & Kinosita, 1981) which reduced the anisotropy values. Theoretically, excitation of as much as 10% of the probe molecules per flash leads to only 4% reduction in anisotropy; our measurements at a few percent of excitation should be free from this effect. In practice, however, the beam inhomogeneity led to local overexcitation which was difficult to assess directly. Moreover, it is the excitation to the singlet state that counts when the flash duration is not much longer than the singlet lifetime (2.2 ns for EMI–myosin in 0.5 M KCl at 20 °C), as with our Nd/YAG laser. Experimentally, we obtained $r(0)$ of 0.38–0.39 for EMI conjugated to *N*-acetyl-L-cysteine and dissolved in glycerol at −20 °C; the excitation level was about 1%, and the beam was carefully adjusted. This $r(0)$ compares with the theoretical maximum of 0.4. From this and other results at higher intensities, we estimate that the absolute anisotropy values reported in this paper may be slightly too low, but the error is within 10%; correction was not attempted since the beam quality changed from time to time. The saturation effect reduces $r(t)$ by a constant factor and does not alter the time dependence (Kawato & Kinosita, 1981). Errors due to the rotation of the plane of polarization by sucrose and the depolarization due to scattering are estimated to be within the 10% range. (Sucrose dramatically reduced the turbidity.)

The EMI–cysteine in glycerol gave a steady-state fluorescence anisotropy of 0.37 upon excitation at 515 nm and observation above 560 nm (excitation at the red edge, 545 nm, gave an anisotropy of 0.38, suggesting a possibility of two overlapping absorption bands with nearly parallel transition moments). Thus, the transition moment for fluorescence emission is almost parallel to the absorption moment. In contrast, $r(0)$ for phosphorescence signal was 0.16, showing that the moment for phosphorescence emission makes an angle of about 39° with the absorption moment.

Estimation of the Viscosity of Sucrose Medium. After each triplet measurement, the sucrose concentration in the sample was estimated from the refractive index measured with an Abbe refractometer; contribution of KCl to the refractive index was subtracted. The viscosity of the medium was then calculated from the sucrose concentration and the measured temperature by using a semiempirical equation by Barber (1966). Although application of the equation to temperatures below 0 °C is not necessarily warranted, our results below, particularly Figure 4, indicate that the equation should be a good approximation.

Due to the oxygen removal procedure, the final sucrose concentration could not be controlled precisely, resulting in a variation of a few percent (w/w). Also in several instances we deliberately changed the concentration by several percent to manipulate the viscosity. To make comparison easier, we report all anisotropy curves in sucrose, in subsequent figures, in such a way as though they had been measured at the nominal sucrose concentration of 60% (w/w) at nominal temperatures, by reducing the horizontal scale in proportion

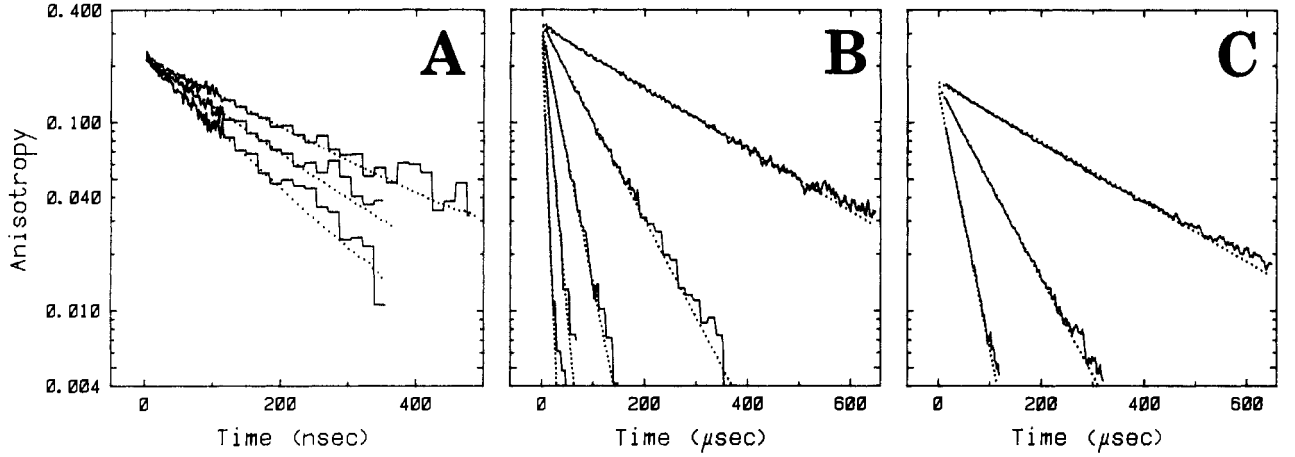

FIGURE 3: Anisotropy decays of labeled S1. (A) Fluorescence anisotropy decays of PMI–S1 at 0 (top), 10 (middle), and 20 °C (bottom) in 0.5 M KCl, 10 mM MOPS, and 0.1 mM EDTA, pH 7.0. [S1] = 8.2 μM. Excitation at 343 nm and emission above 370 nm. (B) Absorption anisotropy decays of EMI–S1 at −20, −10, 0, 10, and 20 °C (from top to bottom) in the same medium plus 5 mM dithiothreitol and sucrose to 60% (w/w). [S1] = 23 μM. (C) Phosphorescence anisotropy decays of EMI–S1 at −20 (top), −10 (middle), and 0 °C (bottom) in the same medium as in (B). [S1] = 2.3 μM. In all panels, the zigzag solid lines are experimental data, and the dotted lines are the best-fit single-exponential curves.

to T/η where T is the absolute temperature and η the viscosity.

Fluorescence Measurements. Time-resolved and steady-state fluorescence measurements were made with a computer-aided photon counting apparatus already described (Kinosita et al., 1981).

Results

Rotational Motion of Isolated S1. Figure 3 shows the decays of anisotropy, $r(t)$, of PMI fluorescence (A), EMI absorption (B), and EMI phosphorescence (C) for labeled S1 in 0.5 M KCl at various temperatures; EMI signals were obtained in 60% (w/w) sucrose since the decays were otherwise too fast. All the anisotropy decay curves could be fitted well with a single exponential function (dotted lines); particularly good signal-to-noise ratio in the triplet signals allowed us to confirm the exponential character over two decades. The presence or absence of MgATP (5 mM $MgCl_2$ and 2 mM ATP), or reduction of KCl concentration to 0.1 M, did not affect the anisotropy decay.

Figure 4 summarizes the relaxation time, ϕ, of anisotropy decay (eq 8 with $M = 1$) for EMI–S1. All data points in the figure fall, within experimental error, on the straight line with a slope of 1, showing that ϕ was proportional to $\eta/(k_BT)$ where k_B is the Boltzmann constant:

$$\phi = V_e\eta/(k_BT) \qquad (9)$$

The coefficient V_e is the volume of equivalent sphere (Yguerabide, 1972) for EMI–S1, and its value was found to be 506 ± 25 nm^3 (standard deviation for all points in Figure 4). The data for PMI–S1 in Figure 3A also satisfied eq 9 with a V_e of 495 ± 8 nm^3. Thus, no gross conformational change of S1, as manifested by V_e changes, was detected in response to changes in temperature (−20 to 20 °C), KCl concentration (0.5 or 0.1 M), or the addition of MgATP.

The volume of an unhydrated S1 molecule is calculated to be 140 nm^3 from the molecular weight of 115 000 and the partial specific volume of 0.74 mL/g (Yang & Wu, 1977). The hydrated volume V_h of S1 will then be between 180 and 310 nm^3, depending on the choice of the degree of hydration between 0.2 (Mendelson et al., 1973) and 0.9 g of H_2O/g of protein (Morel & Garrigos, 1982). The large difference between V_h and the experimental V_e above indicates a nonspherical shape for S1; possible dimer–monomer equilibrium (Morel & Garrigos, 1982) is ruled out under our experimental

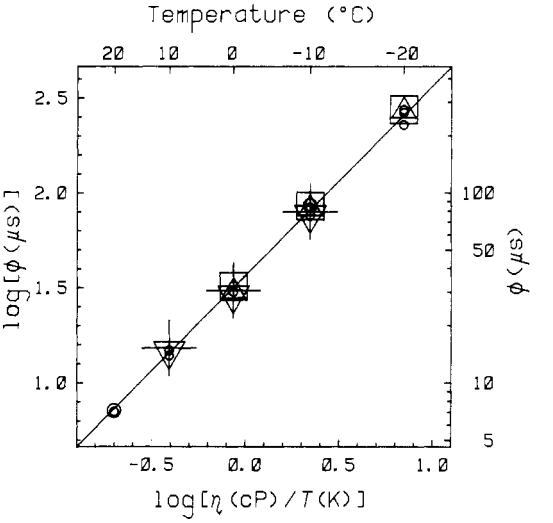

FIGURE 4: Relaxation times, ϕ, for anisotropy decay of EMI–S1 in the sucrose medium. (○) Absorption in 0.5 M KCl; (□) phosphorescence in 0.5 M KCl; (▽) absorption in 0.1 M KCl; (△) phosphorescence in 0.1 M KCl; (+) absorption in 0.5 M KCl plus 5 mM $MgCl_2$ and 2 mM ATP. The straight line shows a relation $\phi = \eta V_e/(k_BT)$ where V_e = 506 nm^3.

conditions since $r(t)$ was single exponential.

Theoretically, an anisotropy decay for an ellipsoid of revolution consists of three exponentials; the parameters involved are the lengths of the principal semiaxes and the orientation of the transition moments of the probe with respect to the axes (Tao, 1969). The decay may be approximated with a single exponential (a) for prolate ellipsoids with either the absorption or emission transition moment of the dye nearly parallel to the symmetry axis or (b) for any oblate ellipsoids. Ellipsoid models consistent with our decay data are listed in Table III. The prolate model with V_h of 180 nm^3 is similar to the least asymmetric model of Mendelson et al. (1973); $r(t)$ of their IAEDANS–S1 gave a V_e of 536 nm^3, which is not very different from our values. Although their $r(t)$ with a limited dynamic range could not eliminate more elongated models, our data over two decades allow more definite estimates. In particular, the largest diameter, which is not very sensitive to the choice of V_h, is unlikely to be much greater than 17 nm.

Since electron microscopy has shown elongated images for the myosin head with a long axis of 15 (Moore et al., 1970) to 21 nm (Takahashi, 1978), most workers have preferred a

Table III: Hydrodynamically Equivalent Ellipsoid of Revolution, with Principal Semiaxes a, b, and b, for Myosin Subfragment 1

	V_h (nm^3)[a]	$2a$ (nm)	$2b$ (nm)	ϵ (deg)[b]
prolate	180	16–17	4.7–4.5	≲20
	310	14–17	6.5–5.8	≲45
oblate	180	2.1	13	
	310	3.9	12	

[a] $V_h = (4\pi/3)ab^2$. [b] The angle between symmetry axis a and the direction of absorption (or emission for PMI) transition moment of the probe.

prolate approximation to oblate [summarized by Wegener (1982)]. We are also tempted to adopt this view. However, the fact that three different probes, PMI, EMI, and IAEDANS, gave similar V_e then suggests that the transition moments, either absorption or emission, of these probes are all within 20–45° of the symmetry axis. This may simply be coincidence or else support for an oblate model suggested by Yang & Wu (1977). Note here that an ellipsoid model is a hydrodynamic equivalent of the real structure; a bent rod, for example, may appear as an oblate ellipsoid if the bend angle is large.

The single exponential $r(t)$'s in Figure 3 also indicate that S1 is rigid, at least over a large part including the probe binding site, SH_1; segmental flexibility would have resulted in a upward concave $r(t)$. The binding site, however, allowed a limited dye wobble, as indicated by the initial anisotropy, $r(0)$, obtained by extrapolation. For EMI absorption, $r(0)$ was about 0.33, which was in reasonable agreement with a steady-state fluorescence anisotropy of 0.34 obtained at 20 °C in the absence of sucrose (excitation at 515 nm and observation above 560 nm). The difference between these values and the anisotropy values for EMI–cysteine in glycerol suggests a wobbling with a semiangle of about 15° for EMI on S1. The angle ϵ in Table III should thus be understood as a time average. Fluorescence anisotropy of EMI–S1 in 60% (w/w) sucrose was 0.37, suggesting that the binding site was accessible to sucrose; subnanosecond dye wobble in water will be slowed down by 2 orders of magnitude in 60% sucrose. The relatively low $r(0)$ of 0.21 for PMI–S1 also suggests some motional freedom for PMI. However, the low anisotropy may be a property of PMI conjugates since PMI bound to H^+-translocating ATPase showed a similar $r(0)$ (Kinosita et al., 1983).

The phosphorescence signal from EMI–S1 gave $r(0)$ of 0.16. Thus, the phosphorescence/absorption anisotropy ratio for EMI-S1 is somewhat higher than the ratio for EMI-cysteine in glycerol (see Materials and Methods). Wobbling of EMI on S1 appears to involve a mode that interchanges the directions of the phosphorescence and absorption transition moments (e.g., rotation about an axis that lies in between the two moments).

In contrast to $r(t)$, neither of the probes gave a single exponential decay for $I_T(t)$ or $\Delta A_T(t)$. Reasonable fits were obtained, for example, with $I_T(t) \propto 0.40 \exp(-t/8.3\ \text{ns}) + 0.33 \exp(-t/45\ \text{ns}) + 0.28 \exp(-t/129\ \text{ns})$ for PMI–S1 at 0 °C or $\Delta A_T(t) = -0.005[0.24 \exp(-t/240\ \mu\text{s}) + 0.76 \exp(-t/1950\ \mu\text{s})]$ for EMI–S1 at 0 °C. The values depended strongly on temperature, and the eosin decay varied to some extent from sample to sample. However, anisotropy decays were always single exponential and were not affected by the variation in the decay kinetics of the excited state.

Effect of Sucrose on the Head Motion in Filaments. The absorption anisotropy decay for synthetic filaments of EMI–myosin in 0.1 M KCl is shown in Figure 5A. In contrast to the signals from the isolated S1, $r(t)$ leveled off after an initial rapid decay, suggesting that the head motion was somewhat restricted in filaments.

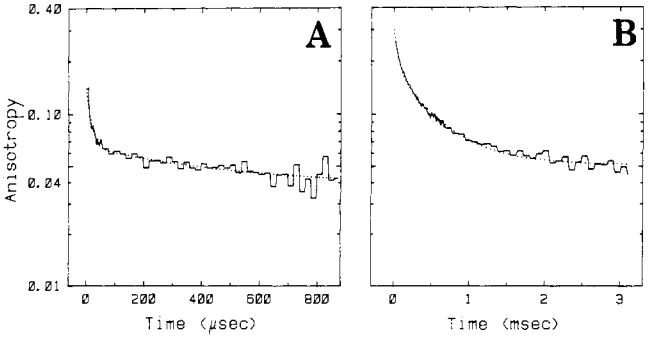

FIGURE 5: Absorption anisotropy decays of EMI–myosin in 0.1 M KCl, 10 mM MOPS, 0.1 mM EDTA, and 5 mM dithiothreitol, pH 7.0 (A) and in the same medium plus sucrose to 60% (w/w) (B), both at 0 °C. [Myosin] = 7.3 μM. The zigzag solid lines are experimental data, and the dotted lines are the best-fit curves for eq 8 in the text with $M = 3$ and $\phi_3 = \infty$.

The initial decay in water was too fast to resolve with our apparatus. We therefore added sucrose and obtained the data shown in Figure 5B. Sucrose slowed down the motion, as in the case of S1, but did not change the final plateau level or the angular range of rotational motion. The addition of sucrose to a final concentration of 60% (w/w) reduced the overall salt concentration to half (to 0.05 mol of KCl/L of sucrose solution). By varying the KCl concentration, however, we found that the same plateau level in anisotropy was obtained in the absence and presence of sucrose when the amount of KCl per water, and not the amount per total volume, was kept constant. Preliminary measurements of turbidity against KCl concentration also suggested that the filament structure was preserved in sucrose when KCl concentration was 0.1 mol/L water and not when it was 0.1 mol/L total volume. When examined under a fluorescence microscope, the sample in Figure 5B showed numerous tiny spots with a size of the order of 1 μm, together with some fluffy materials which were apparently loose clumps of filaments. The amount of the clumps differed from preparation to preparation but did not affect $r(t)$, which reflected motions over distances of the order of nanometers, beyond the experimental error.

The decay kinetics of the triplet excited state, $\Delta A_T(t)$, were similar to those for EMI–S1 and consisted of at least two components, one with a time constant in the microsecond range and the other in milliseconds. Variations of $\Delta A_T(t)$ between samples were observed, but $r(t)$ was reproducible.

Head Motions in HMM, Myosin Monomer, and Filament. Figures 6–8 show the absorption anisotropy decays of EMI–HMM in 0.5 M KCl and EMI–myosin in 0.5 and 0.1 M KCl, all in 60% (w/w) sucrose, at different temperatures. The curves in the left-hand side panels are raw data, showing that the head motion became faster as the temperature was increased. When the time scale of each curve was reduced to that at 20 °C in water by assuming that the rate of rotational motion (and therefore of the anisotropy decay) was proportional to T/η, all curves in each figure essentially overlapped with each other as shown in the right-hand side panels. Thus, there was no gross conformational change in and around the head portion over the temperature range between −10 and 30 °C. Closer examination of the reduced curves suggests that the amplitude of the initial submicrosecond decay became somewhat larger at higher temperatures with a concomitant decrease in the amplitude of the slower (a few microseconds) decay. However, the apparent trend is only barely above the error level.

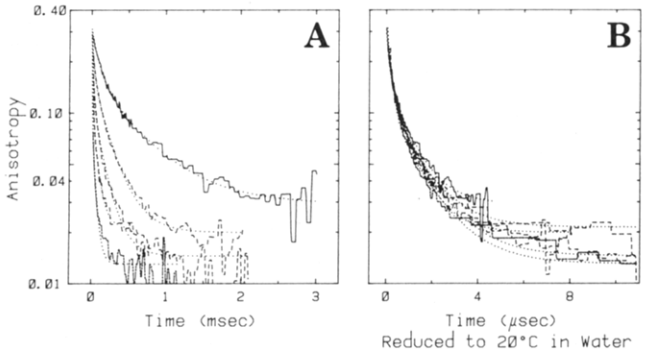

FIGURE 6: Absorption anisotropy decays of EMI–HMM in 0.5 M KCl–sucrose medium (see the legend to Figure 5 for composition). (A) Raw experimental curves at −10, 0, 10, 20, and 30 °C from top right to bottom left (zigzag lines) and the best-fit curves for eq 8 with $M = 3$ and $\phi_3 = \infty$ (dotted lines). (B) The same curves reduced horizontally by a factor of $[(\eta/T)_{20°C\text{ in water}}]/[(\eta/T)_{\text{measured temp in 60\% sucrose}}]$. [HMM] = 4.3 μM.

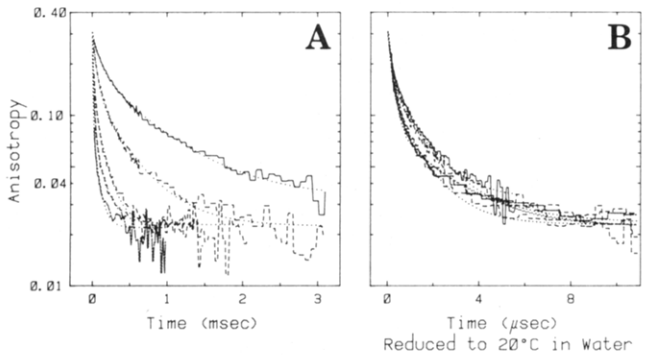

FIGURE 7: Absorption anisotropy decays of EMI–myosin in 0.5 M KCl–sucrose medium. See the legend to Figure 6 for details. [Myosin] = 4.7 μM.

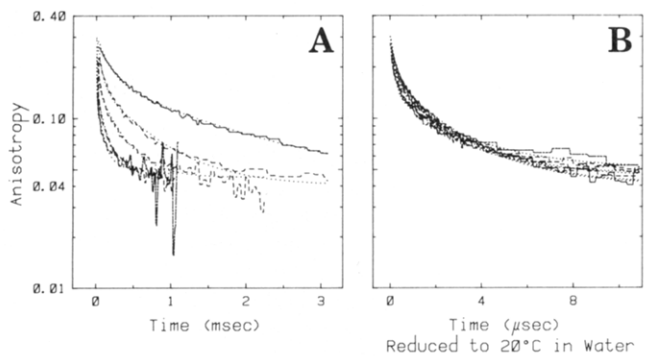

FIGURE 8: Absorption anisotropy decays of EMI–myosin in 0.1 M KCl–sucrose medium. See the legend to Figure 6 for details. [Myosin] = 4.7 or 8.4 μM.

Since the head motion on the reduced time scale was basically independent of temperature, we compare in Figure 9 anisotropy decays in four different systems, myosin filaments in 0.1 M KCl, myosin monomers in 0.5 M KCl, HMM, and S1 at selected temperatures. (The four sets of curves in each panel are in this order from top to bottom.) Figure 9A shows the initial decays at −10 °C, and Figure 9B shows the complete decays at 10 °C, both in the reduced time scale. The fluorescence depolarization studies using IAEDANS (Mendelson et al., 1973; Mendelson & Cheung, 1976, 1978) examined the top-left portion of Figure 9A, where the previous results and ours are basically consistent.

An important feature of Figure 9B, revealed by the very long triplet lifetime, is the extensive decay of anisotropy even in filaments (also see the data in the absence of sucrose, Figure

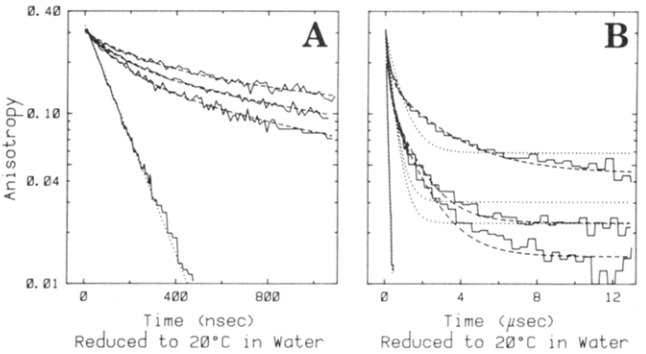

FIGURE 9: Typical absorption anisotropy decays, on the reduced time scale, of EMI–myosin in 0.1 M KCl, EMI–myosin in 0.5 M KCl, EMI–HMM in 0.5 M KCl, and EMI–S1 in 0.5 M KCl (from top right to bottom left), all in the sucrose medium. (A) Initial portions measured at −10 °C. (B) Entire decay curves measured at 10 °C. The solid lines, experimental; the dotted lines, best-fit curves for eq 8 with $M = 2$ and $\phi_2 = \infty$ ($M = 1$ for S1); the dashed lines, best-fit curves for eq 8 with $M = 3$ and $\phi_3 = \infty$.

5A). The myosin heads on the filaments apparently undergo extensive wobbling motion within a time range as short as several microseconds. This is contrary to the prediction by Mendelson & Cheung (1978) that the head motion in synthetic and native filaments is restricted within a cone of semiangle of less than 12.5°. Our data indicate an angular excursion of many tens of degrees; e.g., if the head is assumed to wobble uniformly in a cone, and if the transition moment of EMI is parallel to the head axis, the semiangle of the cone is calculated to be about 60° for the filament data. The wobbling angle should be large for both heads of a myosin molecule, since more than one head per myosin was labeled with EMI (Table I). The large-amplitude wobbling is consistent with the previous findings (Yanagida, 1981; Cooke et al., 1982) that the myosin heads in relaxed muscle assume random orientations. Thomas et al. (1980) have reported a rotational correlation time of the order of 10 μs for spin-labeled myosin heads in synthetic filaments and in relaxed myofibrils.

Quantitative analyses of the decay curves were made with eq 8. The smooth dotted lines in Figure 9B are the best-fit curves based on the exponential-plus-constant approximation (eq 8 with $M = 2$ and $\phi_2 = \infty$), which is clearly inadequate except for S1 which gave a single-exponential decay. Good fits were obtained by adding one more exponential term ($M = 3$, $\phi_3 = \infty$), as seen in the dashed curves (also the dotted lines in Figures 6–8). In the fitting, we fixed the initial anisotropy, r_0, to a value obtained at high time resolution; measurement of the whole decay required a lower resolution, resulting in some degradation of the initial rapid decay. The results of the analyses are summarized in Table IV.

Before interpreting the parameters in Table IV, we estimate the consequence of inhomogeneous labeling: about 8% of EMI was in the rod fraction, as seen in Table I. A rod sample obtained by chymotryptic digestion of labeled myosin, as well as myosin labeled in the presence of excess F-actin which presumably protected SH_1, gave a practically constant anisotropy of 0.16–0.18 in 0.1 M KCl over the time range of Figure 9B (existence of an initial very rapid decay cannot be excluded). The triplet yield and triplet lifetime appeared not much different from those for EMI bound to S1. Thus, correction of the filament data (top row in Table IV) for the rod EMI would increase r_0 to 0.315 [$=(0.303 - 0.17 \times 0.08)/0.92$] and decrease β_3 to about 0.13 (with accompanying increases in β_1 and β_2). In 0.5 M KCl, the rod anisotropy decayed to about 0.04; the major correction would simply be an increase of r_0 to 0.320. We neglect these small corrections,

Table IV: Anisotropy Decay Parameters for EMI–Myosin and Its Subfragments[a]

sample	n	r_0	β_1	ϕ_1 (ns)	β_2	ϕ_2 (ns)	β_3	$\langle\phi\rangle$ (ns)	$\langle\phi^{-1}\rangle$ (μs^{-1})
myosin	18	0.303	0.44	215	0.39	2150	0.17	1100	2.26
0.1 M KCl			(0.07)	(32)	(0.07)	(520)	(0.04)	(180)	(0.39)
myosin	11	0.308	0.57	187	0.35	1640	0.08	717	3.39
0.5 M KCl			(0.10)	(39)	(0.08)	(410)	(0.02)	(121)	(0.68)
HMM	7	0.313	0.55	154	0.40	1160	0.06	569	3.89
0.5 M KCl			(0.08)	(30)	(0.08)	(230)	(0.02)	(38)	(0.38)
S1	12	0.326	1.00	125				125	8.00
0.5 M KCl				(7)				(7)	(0.46)

[a] Data at −10 to 30 °C in 60% (w/w) sucrose were analyzed with eq 8 in the text. The parameter values were averaged after reducing the time constants to 20 °C in water. Numbers in parentheses are the standard deviations over n measurements. Variations in r_0 were within ±0.01. $\langle\phi\rangle \equiv (\beta_1\phi_1 + \beta_2\phi_2)/(\beta_1 + \beta_2)$; $\langle\phi^{-1}\rangle \equiv \beta_1/\phi_1 + \beta_2/\phi_2$.

since the statistical error is already large.

The initial slope of anisotropy decay is proportional to the rate of rotational motion (rotational diffusion constant) irrespective of whether the motion is restricted by a potential or not (Kinosita et al., 1977). Figure 9A then shows that the motion of the head connected to the rod portion was several times slower than the motion of the isolated S1 [the last column in Table IV shows approximate values of normalized initial slope, $(dr/dt)_{t=0}/r_0$]. This result is consistent with the existence of a swivellike joint between the head and the rod portion, as already suggested by Mendelson et al. (1973). Wobbling of the head around the joint, which moves only slowly in space, is naturally slower than the rotation of isolated S1 around its center. The relatively small differences in the initial slopes among filaments, myosin monomers, and HMM suggest that the motion of the joint itself was more restricted in this order.

Wegener (1982) has developed a detailed hydrodynamic theory to calculate the rotational behavior of swivel-jointed myosin models. A typical model consisted of two prolate heads of length 16 nm and width 4.5 nm connected with an isotropic swivel joint to a cylindrical rod of length 144 nm and diameter 2 nm; a second isotropic swivel joint was postulated in the rod portion at 43 nm from the head–rod junction. The end-over-end rotational diffusion constant has been calculated for this and other models (reasonable changes in the dimensions of the rod portion, or even the exclusion of the second swivel, did not alter the diffusion constant of the head by more than 10%). If we, too, assume that the head is prolate rather than oblate, our results can be directly compared to his theory, since our $r(t)$ should then reflect the end-over-end rotation of the head (absorption moment of EMI should in this case be parallel to the major axis, as shown in Table III). For the above model, theoretical values (hereafter, all values refer to 20 °C in water) of normalized initial slope for S1, HMM, and myosin monomer were 8.16, 4.31, and 3.95 μs^{-1}, in good agreement with the experimental values in the last column of Table IV. Theoretical models for filament were not given, but a model in which the head–rod junction was fixed in space gave a slope of 2.97 μs^{-1}. Another model to be compared with the filament data would be one in which the second joint instead of the head–rod junction is fixed in space. This model, although not treated in the theory, can be approximated by one of his models with a rigid and straight rod portion (a cylinder with one end fixed is equivalent to a longer cylinder rotating freely), which gave a slope of 3.68 μs^{-1}. The experimental slope for filament is not very different from these theoretical values. An almost perfect agreement between the experiments and theory may be expected if we assume that the undigested head connected to the rod is slightly ($\lesssim$1 nm) longer than the isolated S1. Note again that the above comparison based on the initial slope is valid even when the joints are not completely isotropic, i.e., in the presence of a restoring force, a situation not explicitly considered in the theory. The possibility of an oblate head was not considered in the theory, but the difference in the slope between the isolated and connected heads should be smaller than in the prolate model (less than 2-fold even when the head–rod junction is fixed in space).

A single swivel at the head–rod junction is not sufficient to account for the anisotropy decays shown in Figure 9B. First of all, it is clear that the swivel cannot be isotropic, since the decay would then be closer to an exponential. There must be a potential barrier, springlike or wall-like, against the head rotation. Wobbling of the head in the barrier, however, cannot explain the relatively slow decay beyond 1 μs (ϕ_2 in Table IV). Theoretical considerations (Kinosita et al., 1977, 1982) have shown that the major effect of a potential barrier on the anisotropy decay is the addition of a constant term: $r(t)$ should be closely approximated with an exponential plus a constant,[2] and the exponential term should have a slope close to the one for the potential-free decay determined by the geometry of the object. The experimental decays deviate markedly from this prediction (see the dotted lines in Figure 9B). We are thus led to a conclusion that the slowly decaying component arises from rotation of an object larger than the head, i.e., from a combined rotation of the head and something attached to it. A natural candidate is the rod portion: We suggest that part of the rod next to the head wobbles extensively even in filaments.

Addition of MgATP (5 mM $MgCl_2$ and 2 mM ATP) or raising the pH to 8 did not change the filament $r(t)$ appreciably. The effect of pH, however, may be worth further study since the pH was changed only after the formation of filaments.

Discussion

Analysis with a Double-Cone Model. Encouraged by the agreement between Wegener's theory and the experimental initial slopes, we propose a model illustrated in Figure 10 as the simplest model that accounts for the essential features of the observed anisotropy decays: A prolate head (the other head is omitted for simplicity) of length L_1 is connected via a swivel joint, which allows a wobbling of the head within a cone of semiangle θ_1, to a stem of length L_2. The stem, in turn, is connected via a similar joint of cone angle θ_2 to the rest of the rod. The head wobbles with a wobbling (=rotational) diffusion constant D_1 and the stem with D_2. The absorption transition moment of EMI is assumed to be parallel to the prolate axis. The axis of cone 1 is assumed to be approximately parallel

[2] This has been shown by direct calculation for the wobbling-in-cone model, in which the potential is of a square-well type (Kinosita et al., 1977). An exponential-plus-constant approximation for a model with a Gaussian (springlike) potential gave an initial slope very close to the correct one (Kinosita et al., 1982), indicating that the approximation is even better for the Gaussian model than for the cone model.

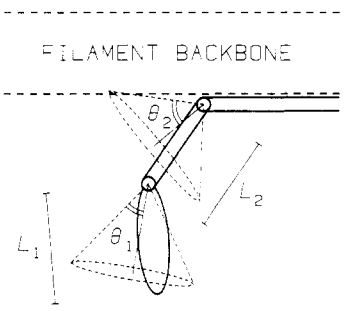

FIGURE 10: Double-cone model for the analysis of the wobbling motion of myosin head. In the figure, $\theta_1 = 35°$, $\theta_2 = 48°$, $L_1 = 16$ nm, $L_2 = 14$ nm, the width of the head = 4.5 nm, and the diameter of the filament backbone = 12 nm.

Table V: Analyses of the Head Motion with the Double-Cone Model[a]

sample	D_1 (μs^{-1})	θ_1 (deg)	D_2 (μs^{-1})	θ_2 (deg)
myosin	0.45	35	0.075	48
0.1 M KCl	(0.07)	(2)	(0.013)	(4)
myosin	0.64	41	0.13	57
0.5 M KCl	(0.13)	(5)	(0.02)	(3)
HMM	0.79	41	0.19	60
0.5 M KCl	(0.06)	(5)	(0.03)	(3)
S1[b]	1.34	180		
0.5 M KCl	(0.02)			

[a] The wobbling parameters were calculated for each temperature from the average values of decay parameters and then averaged. Numbers in parentheses show the standard deviations in the averaging over different temperatures. [b] D_1 is for free rotation of isolated S1.

to the stem axis for the reasons stated in the next subsection.

The wobbling-in-cone calculation (Kinosita et al., 1977) suggests that the anisotropy decay for this model is approximated by

$$r(t)/r_0 = [(1-\gamma_1)\exp(-t/\phi_1) + \gamma_1][(1-\gamma_2)\exp(-t/\phi_2) + \gamma_2] \approx (1-\gamma_1)\exp(-t/\phi_1) + \gamma_1(1-\gamma_2)\exp(-t/\phi_2) + \gamma_1\gamma_2 \quad (\phi_1 \ll \phi_2) \quad (10)$$

provided $D_1 \gg D_2$ (a condition for approximate independence of the two wobbling motions). The parameters γ_i and ϕ_i are related to θ_i and D_i, under the assumption of $D_1 \gg D_2$, by

$$\gamma_i = [\cos\theta_i(1+\cos\theta_i)]^2/4 \qquad \phi_i = \sigma_i/D_i \quad (11)$$

where σ_i is a known function of θ_i (Kinosita et al., 1977).

Equation 10 for $\phi_1 \ll \phi_2$ has the same form as the equation used for the analysis of experimental $r(t)$, and Table IV shows that the condition $\phi_1 \ll \phi_2$ (and therefore $D_1 \gg D_2$) is fulfilled. Thus, we can estimate θ_i and D_i from the parameter values in Table IV. The results are shown in Table V. Both the head and stem wobble over many tens of degrees.

Since D_1 determines the initial slope ($\approx 6D_1$) of $r(t)/r_0$ under the condition of $D_1 \gg D_2$, the values for D_1 in Table V agree with Wegener's theory as expected: Theoretical D_1 values for isolated S1, HMM, myosin monomer, and head fixed at one end are respectively 1.36, 0.72, 0.66, and 0.49 μs^{-1}, for the head dimensions of 16 nm ($=L_1$) × 4.5 nm. The experimental D_1 for filament may appear somewhat too small, since the head–stem junction is not fixed in our model, but the experimental error is large. The interaction with the filament backbone might also account for the small discrepancy.

D_2 may be translated into L_2, the length of the stem, if we approximate the stem with a cylinder of diameter 2 nm (the discussion below is not sensitive to the value of the diameter). Cylinders with one end fixed and with a length of 25 or 30 nm will have a wobbling diffusion constant of 0.10 or 0.066 μs^{-1}, respectively (Yu & Stockmayer, 1967). These values are to be compared with the filament D_2 in Table V (top row). Thus, if we ignore the heads, L_2 will be slightly less than 30 nm, which is the upper limit for L_2. Presence of the heads makes estimation difficult, but we expect that L_2 is about 30 − 16 ($=L_1$) = 14 nm. For myosin monomer and HMM, Wegener (1982) has calculated the end-over-end rotational diffusion constant of the stem portion of length 43 nm to be 0.032 and 0.088 μs^{-1}, respectively. Although his models assume isotropic rotation of the heads, these values are too small compared to D_2 in Table V, suggesting that L_2 should be smaller than 43 nm.

The value for L_2 is considerably smaller than the length of subfragment 2 (a part of the rod next to the heads; obtained by enzymatic digestion), either 43 or 65 nm depending on digestion conditions (Sutoh et al., 1978). According to Highsmith et al. (1977), the long subfragment 2 is flexible. Tsong et al. (1979) have shown a partial melting of the α-helical structure of subfragment 2 at physiological temperature. Electron micrographs of quick-frozen, deep-etched, unfixed insect flight muscle in rigor have revealed a narrow stalk of diameter about 3 nm between the backbone of thick filament and a bulbous "head"; the stalks were observable when the cross bridges spanned perpendicularly the gap between the thick and thin filaments under conditions which produced an unusually wide gap of ≳20 nm (Heuser & Cooke, 1983).

Examination of the Assumptions in the Model. In the following we attempt to evaluate the various assumptions and statements made in the preceding subsection.

(*i*) *Is a Well-Defined Swivel Joint Present at the Head–Rod Junction*? The alternative would be a distributed flexibility over a considerable length around the junction region. However, (a) the head itself, at least a large part containing SH_1, appears rigid (Figure 3). (b) A very flexible junction chain with a length comparable to or greater than the head dimensions is unlikely, as pointed out by Mendelson et al. (1973), since the initial slope of anisotropy decay would then be similar to the one for free S1. (c) If the head–rod junction allows only a very limited head wobble, as Mendelson & Cheung (1978) suggested, and further rotation requires a rather uniform bend of a considerable length of rod end, the anisotropy decay would have slowed down at a point earlier than shown in Figure 9. The excellent fit of experimental $r(t)$ with eq 10 and the agreement between D_1 and Wegener's results strongly indicate a short swivellike junction that allows a head wobble to the extent of θ_1 in Table V.

(*ii*) *Swivel or Hinge and Wall or Spring*? If the head–rod junction is hingelike, β_1 in Table IV would suggest a swing angle in a plane of ±45° for filament and even a larger angle for myosin monomer and HMM. It is difficult to imagine that such an extensive motion in the narrow joint is limited only in one direction, although the complete axial symmetry of the cone model may well be an oversimplification (θ_1 should then be taken as an average). As to the shape of the potential against the head wobble, we cannot discriminate between the square-well type, as in the cone model, and a Gaussian, springlike one, since they give similar anisotropy decays (Kinosita et al., 1982). If the potential is Gaussian, θ_1 in Table V represents the angular range in which the head axis resides for 86% of the time (Kawato & Kinosita, 1981; Kinosita et al., 1982).

(*iii*) *Is the Head Prolate Rather Than Oblate*? The data on isolated S1 cannot discriminate between the two possibilities, but the agreement of the initial slopes with Wegener's theory is better for prolate than for oblate models.

(*iv*) *Does the Fast-Decaying Component in r(t) Originate Entirely from Head Wobble*? If the transition moment of

EMI makes a large angle with the head axis that passes through the center of the head and the head–rod junction, rotation of the head around this axis also decreases anisotropy. This situation is unlikely for a prolate head where the moment should be nearly parallel to the long axis (Table III), unless the junction site is close to the equator of the prolate head. An oblate head, on the other hand, might fit the situation. A major difficulty, however, is that the rate of the axial rotation, in contrast to the rate of wobbling, is not sensitive to whether the head is free or connected to the rod portion. Since we do not see, in the top three sets of curves in Figure 9A, any sign of a component that decays with a slope comparable to the one in the bottom curve, we believe that there is no contribution from the axial rotation. It might also be argued that the reduced slopes in the top three curves could be due to a possible difference in the length of the head axis between the isolated and undigested heads. This difference would then be large, at least 2-fold, since the rate of axial rotation is much less sensitive to the length than the wobbling rate. We thus conclude that even if the head is oblate, the EMI moment is collinear with the head axis, and the fast decay reflects the head wobbling.

(*v*) *Does the Slowly Decaying Component Necessarily Reflect the Motion in the Rod Part*? An alternative could be that some kind of friction at the joint (or between two heads or between the head and rod) makes the head motion slow. If this were the case, the rate of anisotropy decay would be determined by the intramolecular friction. The fact that the decay curves are superimposed with each other on the reduced time scale (Figures 6–8) would then imply that the intramolecular friction happens to be proportional to the solvent viscosity over the range of temperature and sucrose concentration examined. Such a coincidence is unlikely, since the change in sucrose viscosity was quite large (e.g., 583 cP at −10 °C at 60%, 58.5 cP at 20 °C at 60%, and 28.1 cP at 20 °C at 55%). The slow decay must have come from a combined motion of the head and something attached to it.

(*vi*) *Is There a Distinct Swivel Joint at L_2 in the Rod*? The existence of a second swivel in Figure 10 is hypothesized for mathematical simplicity. Another possibility is that the rod end is bent rather uniformly. Then, L_2 should be understood as the effective length.

(*vii*) *Is the Axis of Cone 1 Parallel to the Stem*? This assumption is as yet unsupported. Since myosin has two heads, exact parallelism cannot be expected, although a considerable overlap of the two cones for the two heads is conceivable. If the axis of cone 1 is perpendicular to the stem portion, the axial rotation of the stem leads to reorientation of the cone 1 and therefore to a decrease in anisotropy. This reorientational process should be as fast as the wobbling of the head in cone 1, since the friction against the axial rotation of the stem is very weak and the major resistance comes from the heads. [The diffusion constant for axial rotation of a cylinder of length 144 nm and diameter 2 nm (straight myosin rod) is calculated, according to Broersma (1960), to be as large as 2.2 μs^{-1}.] Thus, some of the amplitude of the fast-decaying component may be due to the axial rotation (or twisting) of the stem, but the latter cannot account for the slower component. Since a complete turn of a perpendicular head around the stem axis would decrease anisotropy as much as 4-fold, the values of β_1 for myosin monomer and HMM in Table IV suggest less inclined heads. Then, the axial rotation essentially widens cone 1 and makes the cone axis parallel to the stem. The small difference in θ_1 in Table V between filament and solubilized proteins may reflect this situation.

Dynamic Structure of Muscle Proteins and the Mechanism of Contraction. Our preliminary experiments on myofibrils have indicated that myosin heads in relaxed myofibrils undergo rapid and extensive thermal wobbling which is quite similar, if not exactly the same, to the one in synthetic filaments. Actin filaments also exhibit some bending flexibility, as shown by quasi-elastic light scattering (Fujime & Ishiwata, 1971; Ishiwata & Fujime, 1972) and more recently by direct observation of bending motions under a dark-field microscope (Nagashima & Asakura, 1980) and a fluorescence microscope (Yanagida et al., 1984). F-Actin appears to be even more flexible in the direction of twist: triplet anisotropy decay measurements have revealed a microsecond internal motion which has been assigned to torsional motion of the filament (Mihashi et al., 1983; Yoshimura et al., 1984). The triplet observation is consistent with the electron microscopic analysis by Egelman et al. (1982) which indicated a very high torsional flexibility of actin filaments. We expect that these rapid and extensive thermal motions must play essential roles in the mechanism of muscle contraction.

An immediate consequence of the rapid and extensive wobbling of myosin heads is that the heads undergo a displacement of the order of a few tens of nanometers in a matter of microseconds. Thus, the heads make continual searches for a binding site(s) on the thin filament from various directions and with different orientations. The searches are not very efficient in that they are made in a random fashion, but the high frequency may well make up for the inefficiency. Once the binding sites become available, the heads attach to the thin filament via thermal motions. The model of Huxley & Simmons (1971) involves multiple binding sites between a head and thin filament. The model assumes that the first attachment is made only to the weakest binding site, possibly because an unattached head keeps a particular orientation(s) that does not allow binding to high-affinity sites. This assumption is not compatible with our results, which would suggest indiscriminate attachments, unless one further postulates that the second and subsequent bindings are made possible only after a conformational change induced by the first binding. Such a postulate was not part of (nor required in) the original model.

An elastic component(s) is involved in the contraction mechanism of striated muscles (Huxley & Simmons, 1972). The force against the head wobble appears too weak to be the candidate for the elastic force, since the average thermal energy is sufficient to reorient the head by many tens of degrees. A possibility, however, remains that the potential is steep at the wobble limits (as in the cone model); then, inclination beyond the cone angles shown in Table V could store a considerable amount of elastic energy, far above the level of the average thermal energy.

The two-swivel model in Figure 10 suggests that the translational movement of the head is also relatively free. An effective "pull" against the elastic force thus requires that the wobbling motion ceases once the head is attached to the thin filament, which appears to be the case (Thomas et al., 1980; Yanagida, 1981; Cooke et al., 1982). Our triplet study (unpublished results) has also shown that the attachment is rigid and the microsecond head wobble is absent on actin filament.

Added in Proof

While we were preparing this paper, we received a preprint of the work by Eads et al. (1984). They reported triplet anisotropy experiments similar to ours except that the label was 5-eosinyliodoacetamide instead of EMI. Furthermore, sucrose was absent in their medium. Their results agree quantitatively with ours in Table IV, after appropriate re-

duction in time scale. [Their r_0 values are lower, due presumably to the saturation effect and/or depolarization resulting from light scattering. In our hands, 5-eosinyliodoacetamide, conjugated with L-cysteine and dissolved in glycerol at −20 °C, gave $r(0)$ for absorption of at least 0.38, comparable to the value for EMI. Phosphorescence $r(0)$ and steady-state fluorescence anisotropy values were lower than those for EMI, but the differences were 0.01–0.02. Binding of 5-eosinyliodoacetamide to the myosin head was almost as tight as EMI, since fluorescence anisotropy of the label conjugated with S1 was about 0.31 or higher.] Eads et al. (1984) have also interpreted their results in terms of the double cone model; their values for the diffusion constants and cone angles arre similar to ours in Table V.

Acknowledgments

We thank Dr. K. Mihashi and Dr. S. Kawato for stimulating and helpful discussions. The YAG laser and LSI-11/23 computer for the triplet apparatus were provided by Dr. Kawato, with whom we share the apparatus. Dr. H. Nakane kindly made his refractometer available to us. Dr. D. D. Thomas sent us preprints of their work prior to publication. Help in constructing the triplet apparatus from the workshop at the Institute of Physical and Chemical Research, Sigma Koki Co., Ltd., and Hamamatsu Photonics Co., Ltd., is greatly acknowledged.

References

Ando, T. (1978) in *Lecture Notes for International Summer School of Biophysics* (Yanagida, T., Ed.) pp 145–148, ISSB Committee at Osaka University, Osaka.

Barber, E. J. (1966) *Natl. Cancer Inst. Monogr. No. 21*, 219–239.

Broersma, S. (1960) *J. Chem. Phys. 32*, 1626–1631.

Cherry, R. J. (1978) *Methods Enzymol. 54*, 47–61.

Cooke, R., Crowder, M. S., & Thomas, D. D. (1982) *Nature (London) 300*, 776-778.

Eads, T. M., Thomas, D. D., & Austin, R. H. (1984) *J. Mol. Biol.* (in press).

Egelman, E. H., Francis, N., & DeRosier, D. J. (1982) *Nature (London) 298*, 131–135.

Fujime, S., & Ishiwata, S. (1971) *J. Mol. Biol. 62*, 251–265.

Gornall, A. G., Bardawill, C. J., & David, M. M. (1949) *J. Biol. Chem. 177*, 751–766.

Heuser, J. E., & Cooke, R. (1983) *J. Mol. Biol. 169*, 97–122.

Highsmith, S., Kretzschmar, K. M., O'Konski, C. T., & Morales, M. F. (1977) *Proc. Natl. Acad. Sci. U.S.A. 74*, 4986–4990.

Holowka, D. A., & Hammes, G. G. (1977) *Biochemistry 16*, 5538–5545.

Huxley, A. F. (1957) *Progr. Biophys. Biophys. Chem. 7*, 255–318.

Huxley, A. F., & Niedergerke, R. (1954) *Nature (London) 173*, 971–973.

Huxley, A. F., & Simmons, R. M. (1971) *Nature (London) 233*, 533–538.

Huxley, A. F., & Simmons, R. M. (1972) *Cold Spring Harbor Symp. Quant. Biol. 37*, 669–680.

Huxley, H. E. (1969) *Science (Washington, D.C.) 164*, 1356–1366.

Huxley, H. E., & Hanson, J. (1954) *Nature (London) 173*, 973–976.

Ikegami, A., Kinosita, K., Jr., Kouyama, T., & Kawato, S. (1982) in *Structure, Dynamics, and Bioenergetics of Biomembranes* (Sato, R., & Ohnishi, S., Eds.) pp 1–32, Japan Scientific Societies Press, Tokyo.

Ishiwata, S., & Fujime, S. (1972) *J. Mol. Biol. 68*, 511–522.

Jovin, T. M., Bartholdi, M., Vaz, W. L. C., & Austin, R. H. (1981) *Ann. N.Y. Acad. Sci. 366*, 176–196.

Kawato, S., & Kinosita, K., Jr. (1981) *Biophys. J. 36*, 277–296.

Kinosita, K., Jr., Kawato, S., & Ikegami, A. (1977) *Biophys. J. 20*, 289–305.

Kinosita, K., Jr., Kataoka, R., Kimura, Y., Gotoh, O., & Ikegami, A. (1981) *Biochemistry 20*, 4270–4277.

Kinosita, K., Jr., Ikegami, A., & Kawato, S. (1982) *Biophys. J. 37*, 461–464.

Kinosita, K., Jr., Ikegami, A., Yoshida, M., & Kagawa, Y. (1983) *J. Biochem. (Tokyo) 92*, 2043–2046.

Kinosita, K., Jr., Kawato, S., & Ikegami, A. (1984) *Adv. Biophys. 17*, 147–203.

Koretz, J. F. (1982) *Methods Enzymol. 85*, 20–55.

Kouyama, T., Kimura, Y., Kinosita, K., Jr., & Ikegami, A. (1981) *FEBS Lett. 124*, 100–104.

Lachish, U., Shafferman, A., & Stein, G. (1976) *J. Chem. Phys. 64*, 4205–4211.

Laemmli, U. K. (1970) *Nature (London) 227*, 680–685.

Lowey, S., Slayter, H. S., Weeds, A. G., & Baker, H. (1969) *J. Mol. Biol. 42*, 1–29.

Margossian, S. S., & Lowey, S. (1982) *Methods Enzymol. 85*, 55–71.

Mendelson, R. A., & Cheung, P. (1976) *Science (Washington, D.C.) 194*, 190–192.

Mendelson, R., & Cheung, P. H.-C. (1978) *Biochemistry 17*, 2139–2148.

Mendelson, R. A., Morales, M. F., & Botts, J. (1973) *Biochemistry 12*, 2250–2255.

Mihashi, K., Yoshimura, H., Nishio, T., Ikegami, A., & Kinosita, K., Jr. (1983) *J. Biochem. (Tokyo) 93*, 1705–1707.

Moore, P. B., Huxley, H. E., & DeRosier, D. J. (1970) *J. Mol. Biol. 50*, 279–295.

Morel, J. E., & Garrigos, M. (1982) *Biochemistry 21*, 2679–2686.

Nagashima, H., & Asakura, S. (1980) *J. Mol. Biol. 136*, 169–182.

Ohnishi, S. T., & Barr, J. K. (1978) *Anal. Biochem. 86*, 193–200.

Ohnishi, T., Gall, R. S., & Mayer, M. L. (1975) *Anal. Biochem. 69*, 261–267.

Perry, S. V. (1955) *Methods Enzymol. 2*, 582–588.

Pollack, G. H. (1983) *Physiol. Rev. 63*, 1049–1113.

Reedy, M. K., Holmes, K. C., & Tregear, R. T. (1965) *Nature (London) 207*, 1276–1280.

Sekine, T., & Kielley, W. W. (1964) *Biochim. Biophys. Acta 81*, 336–345.

Sutoh, K., Sutoh, K., Karr, T., & Harrington, W. F. (1978) *J. Mol. Biol. 126*, 1–22.

Takahashi, K. (1978) *J. Biochem. (Tokyo) 83*, 905–908.

Tao, T. (1969) *Biopolymers 8*, 609–632.

Thomas, D. D., Ishiwata, S., Seidel, J. C., & Gergely, J. (1980) *Biophys. J. 32*, 873–890.

Thomas, D. D., Cooke, R., & Barnett, V. A. (1983) *J. Muscle Res. Cell Motil. 4*, 367–378.

Tonomura, Y., Appel, P., & Morales, M. F. (1966) *Biochemistry 5*, 515–521.

Tsong, T. Y., Karr, T., & Harrington, W. F. (1979) *Proc. Natl. Acad. Sci. U.S.A. 76*, 1109–1113.

Wakabayashi, T., & Toyoshima, C. (1981) *J. Biochem. (Tokyo) 90*, 683–701.

Weeds, A. G., & Pope, B. (1977) *J. Mol. Biol. 111*, 129–157.

Wegener, W. A. (1982) *Biopolymers 21*, 1049–1080.

Yanagida, T. (1981) *J. Mol. Biol. 146*, 539–560.
Yanagida, T., Nakase, M., Nishiyama, K., & Oosawa, F. (1984) *Nature (London) 307*, 58–60.
Yang, J. T., & Wu, C.-S. C. (1977) *Biochemistry 16*, 5785–5789.
Yguerabide, J. (1972) *Methods Enzymol. 26*, 498–578.
Yoshimura, H., Mihashi, K., Nishio, T., Kinosita, K., Jr., & Ikegami, A. (1984) *J. Mol. Biol.* (in press).
Yu, H., & Stockmayer, W. H. (1967) *J. Chem. Phys. 47*, 1369–1373.

Effects of Interchain Disulfide Cross-Links on the Trypsin Cleavage Pattern and Conformation of Myosin Subfragment 2†

Renné Chen Lu* and Sherwin S. Lehrer*

ABSTRACT: The ability of 5,5′-dithiobis(2-nitrobenzoate) (Nbs_2) to produce interchain disulfide cross-links in both the long and short forms of myosin subfragment 2 (S2) and the conformational effects of these cross-links have been investigated. Short S2 (residues 3–287) contains two pairs of Cys residues at positions 66 and 108, and long S2 (residues 1–440) contains an additional pair at position 410. The reaction kinetics of each form of S2 with Nbs_2 was biphasic. During the fast kinetic phase the reaction resulted in un-cross-linked species having Nbs-blocked Cys. During the slow phase disulfide-cross-linked species were formed via interchain S-Nbs/SH exchange. For short S2, Cys-66 appeared to react without forming disulfide cross-links, and the Cys-108 pair reacted with partial cross-linking. For long S2, the Cys-66 pair appeared to react with partial cross-linking, and the Cys pairs at 108 and 410 reacted with complete cross-linking. Mild tryptic digestion of disulfide-cross-linked long S2, under conditions that resulted in partial production of short S2 from un-cross-linked LS2, produced peptides T_{1a} and T_{1b} (residues 1 to ~360), with one and two disulfide cross-links, respectively. Further digestion of cross-linked long S2 or cross-linked short S2 resulted in the same shorter fragment, T_2, with an NH_2-terminus beginning at 103 consistent with a sequence of residues 103–287. Circular dichroism studies on long S2 indicated that the presence of disulfide cross-links changed the thermal unfolding profile of the helix. A destabilizing pretransition was observed between 25 and 40 °C for the cross-linked long S2. These studies indicate that interchain disulfide cross-links can create new proteolytic cleavage sites located far from the cross-links as a result of increased destabilization.

Each of the two heavy chains of the myosin molecule consists of an N-terminal globular head portion [S1, M_r(chain) ~100 000] that contains the adenosinetriphosphatase (ATPase) and actin binding sites and a rodlike coiled-coil portion [rod, M_r (chain) ~130 000], the C-terminal part of which [LMM,[1] M_r (chain) ~70 000] forms the core of the thick filament. Most current models of muscle contraction associate the force generation with one or more states which differs in the disposition of the heads relative to the rod (Huxley, 1969; Huxley & Simmons, 1971; Eisenberg et al., 1980). Another force-generating mechanism which has been suggested involves a conformational change in the S2 portion of the rod, i.e., the portion between the heads and LMM (Harrington, 1971, 1979). Localized helix–coil transition (melting) in the rod near the LMM–S2 junction has been interpreted as supporting this concept (Tsong et al., 1983; Swenson & Ritchie, 1980).

Studies with tropomyosin, the prototype of a coiled-coil α-helical molecule, have produced evidence for regions of localized melting (Woods, 1969, 1976; Satoh & Mihashi, 1972; Chao & Holtzer, 1975; Lehrer, 1978; Graceffa & Lehrer, 1980; Potekhin & Privalov, 1982; Betteridge & Lehrer, 1983). The extent of the localized unfolding has been shown to increase upon the introduction of an interchain disulfide bond possibly as a consequence of steric strain (Lehrer, 1975, 1978). This increased unfolding in disulfide-cross-linked tropomyosin appears to be related to an increase in tryptic cleavage at certain sites (Gorecka & Drabikowski, 1977; Ueno, 1984).

Two forms of S2, long S2 (LS2) and short S2 (SS2), can be prepared by proteolytic digestion of myosin (Weeds & Pope, 1977; Highsmith et al., 1977; Sutoh et al., 1978). LS2 spans the whole length between the head/rod junction and the heavy meromyosin/LMM junction, whereas SS2 includes two-thirds of the N-terminal portion of LS2 (Lu, 1980). In the present work we studied the reaction of Nbs_2 with both forms of S2, and we found that disulfide cross-links were produced in both cases. Furthermore, as a result of these cross-links, trypsin produced a different pattern of cleavage. For disulfide-cross-linked LS2, the initial cleavage site near residue 360 and the new secondary cleavage site at Arg-102 are probably due to the presence of disulfide bonds at positions 410 and 108, respectively. Circular dichroism studies of LS2 in the 25–40 °C temperature range indicated an increased unfolding pretransition when the cross-links were present. These studies

† From the Department of Muscle Research, Boston Biomedical Research Institute, and the Department of Neurology, Harvard Medical School, Boston, Massachusetts 02114. *Received April 30, 1984.* Supported by grants from the National Institutes of Health (HL22461, AM28401, and 507 RR05711) and from the American Heart Association (81 767) and by the Muscular Dystrophy Association. A preliminary report has been presented (Lu & Lehrer, 1984).

* Address correspondence to either author at the Department of Muscle Research, Boston Biomedical Research Institute, Boston, MA 02114.

[1] Abbreviations: Nbs_2, 5,5′-dithiobis(2-nitrobenzoate); SS2, short subfragment 2; LS2, long subfragment 2; LMM, light meromyosin; Tris-HCl, tris(hydroxymethyl)aminomethane hydrochloride; EDTA, ethylenediaminetetraacetic acid; Hepes, 4-(2-hydroxyethyl)-1-piperazineethanesulfonic acid; SDS–PAGE, sodium dodecyl sulfate–polyacrylamide gel electrophoresis; bicine, *N,N*-bis(2-hydroxyethyl)glycine.

0006-2960/84/0423-5975$01.50/0